buildings

MDPI

Article

Numerical Approach to Determine the Resistance of Threaded Anchors in Ultra-High-Performance Fiber-Reinforced Cementitious Composite †

Antonina Hochuli [1,*] and Eugen Brühwiler [2]

[1] Transport and Mobility Laboratory, Institute of Structural Engineering, Swiss Federal Institute of Technology (EPFL), 1015 Lausanne, Switzerland
[2] Institute of Structural Engineering, Swiss Federal Institute of Technology (EPFL), 1015 Lausanne, Switzerland; eugen.bruehwiler@epfl.ch
* Correspondence: antonina.hochuli@epfl.ch

† This paper is an extended version of our paper published in Hochuli, A.; Brühwiler, E. Numerical Simulation of the Structural Behavior of Threaded Anchors in UHPFRC. In Proceedings of the 3rd International Interactive Symposium on Ultra-High-Performance Concrete, Wilmington, DE, USA, 4–7 June 2023; and Hochuli, A.; Brühwiler, E. Failure Mechanism of Threaded Anchors in UHPFRC as Simulated by Finite Element Analysis. In Proceedings of the 4th International Symposium on Ultra-High Performance Fibre -Reinforced Concrete (UHPFRC), Menton, France, 21–23 October 2024.

Abstract: Due to their relatively high tensile strength and dense matrix, UHPFRCs have proven to be a highly effective building material for both strengthening existing reinforced concrete structures and constructing new ones. In both cases, the use of fasteners is prevailing, with threaded anchors being frequently employed. The thicknesses of structural components made of UHPFRCs are relatively thin, i.e., at least 30 mm, typically 50 to 100 mm, and exceptionally 100 to 200 mm. Therefore, the aim is to use fasteners with short anchorage lengths. In this study, the structural behavior of a short threaded anchor with a 20 mm diameter and an embedment length of 50 mm (2.5 Ø) in a UHPFRC is investigated using non-linear finite element models. The UHPFRC is assumed to exhibit tensile strain-hardening behavior, with tensile strengths of 7 MPa and 11 MPa, respectively. The modeled anchor was subjected to a continuously increasing uniaxial pull-out force. The results indicate that the fracture mechanism of threaded anchors in UHPFRCs is primarily characterized by the formation of a tensile membrane within the UHPFRC, which acts as the main resisting element against the pull-out force. Additionally, the influence of the UHPFRC's tensile properties on the pull-out behavior and ultimate resistance of the threaded anchors was determined.

Keywords: short anchorage; threaded anchor; numerical simulation; structural behavior; pull-out force

check for updates

Citation: Hochuli, A.; Brühwiler, E. Numerical Approach to Determine the Resistance of Threaded Anchors in Ultra-High-Performance Fiber-Reinforced Cementitious Composite. *Buildings* **2024**, *14*, 3669. https://doi.org/10.3390/buildings14113669

Academic Editor: Alberto Taliercio

Received: 25 September 2024
Revised: 12 November 2024
Accepted: 14 November 2024
Published: 18 November 2024

Copyright: © 2024 by the authors. Licensee MDPI, Basel, Switzerland. This article is an open access article distributed under the terms and conditions of the Creative Commons Attribution (CC BY) license (https://creativecommons.org/licenses/by/4.0/).

1. Introduction

1.1. Industrial Demands and Research Motivation

The use of Ultra-High-Performance Fiber-Reinforced Cementitious Composites (UHPFRCs) in structural engineering, particularly for constructing thin structural elements such of façades, bridges, and highly stressed fixed railway tracks, has revealed a need for anchorage systems with short embedment lengths. Current commercial anchorage systems were originally designed for concrete applications, with a minimum length of 80 mm, which is non-applicable for the constructive design of UHPFRC structural elements with thicknesses between 30 mm and 100 mm.

A recent application in the domain of fixed railway tracks [1] involved replacing damaged concrete monoblocs with a 24 cm height by 11.9 cm thin UHPFRC pedestals after only 40 years of operation. A comparison of project variants showed that due to its relatively high mechanical strength and durability, a UHPFRC can provide significantly more effective engineering solutions, both economically and technically, compared to

traditional reinforced concrete. One of the challenges in this project was to define rail fasteners that were compatible with the entire fastening system. These fasteners had to be 20 mm in diameter but required a short embedment length. Additionally, the pull-out resistance of the anchorage in the UHPFRC had to be determined. This project highlighted the need to further investigate the pull-out resistance of short anchors to optimize UHPFRC-based fixed railway track systems.

Moreover, the mentioned minimal anchor embedment length of 80 mm in concrete presupposes anchoring within the reinforcement layer near the surface. The pull-out resistance of such anchors in concrete has been well studied through numerous laboratory tests and investigations, resulting in four main fracture modes [2]: (a) pull out of a concrete cone, (b) fracture of the anchor, (c) pull out of the anchor, and (d) combined fracture of the concrete cone and anchor pull out.

Since UHPFRCs have significantly different properties from concrete, particularly in terms of tensile strength, fatigue resistance, and ductile deformation behavior, the fracture modes shown in Figure 1 for concrete cannot be directly adopted for the UHPFRC.

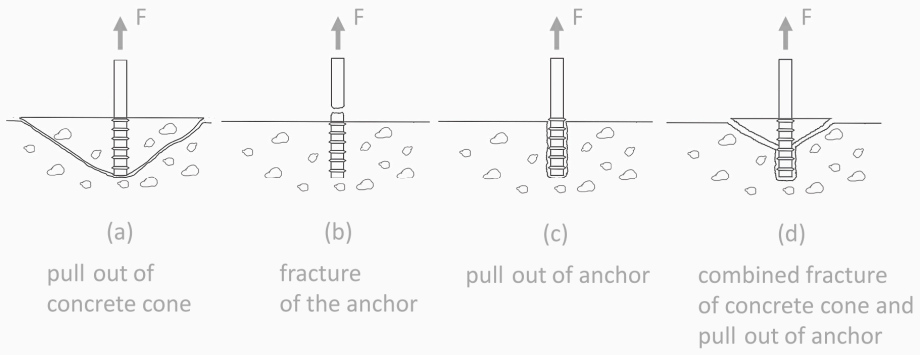


Figure 1. Schematic presentation of the fracture modes of cast-in-place threaded steel anchors in concrete or cementitious material with low tensile strength according to [2].

1.2. Research Objective

The main objective of this research is to investigate the structural behavior of a UHPFRC under quasi-static, continuously increasing forces applied to short threaded anchors. This will be achieved by using non-linear finite element analysis as the first step in the investigation process.

To the best of the author's knowledge, no study is currently available on the structural behavior and pull-out resistance of UHPFRCs with tensile properties, as shown in Figure 1, for anchors with short embedment lengths subjected to pull-out loading.

2. Materials and Methods

2.1. UHPFRC Material Properties

The Ultra-High-Performance Fiber-Reinforced Cementitious Composite is composed of a cementitious matrix with an optimized high packing density, which is strengthened by a high amount of short, slender steel fibers. It has a compressive strength of more than 150 MPa and a tensile strength of more than 12 MPa while developing pronounced tensile strain-hardening and strain-softening behaviors [3]. A further relevant property of the UHPFRC is its extremely low permeability to water, leading to a highly durable material.

The UHPFRC responses to tension (Figure 2) and compression are fundamentally different. Under direct compression, the material remains quasi-elastic almost until reaching the compressive strength. Under direct tension, three domains of material behavior are observed: (1) the elastic domain until the elastic limit stress f_{Ute} is reached, (2) beyond, quasi-linear strain hardening occurs when matrix discontinuities form until the tensile strength f_{Utu} is attained, and (3) gradual softening of a single discrete crack in the weakest cross-section of the specimen, finally leading to material fracture. The fracture zone (3) is a

transitional regime of a so-called fictitious crack, developing from a continuum to a real (stress-free) crack.

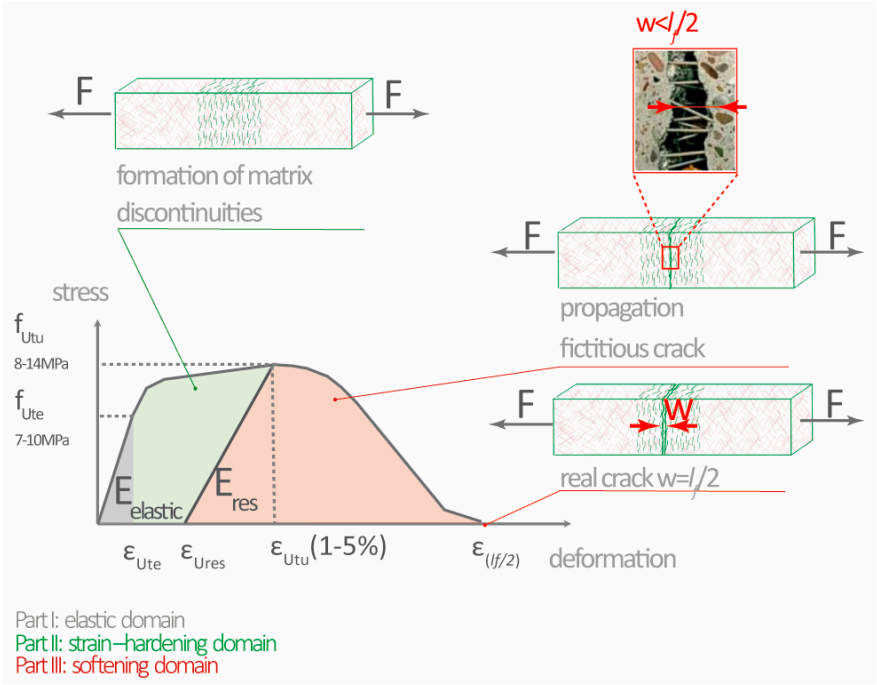


Figure 2. Tensile response of UHPFRC.

In addition, the fatigue endurance limit has been determined to be at a maximum fatigue stress level of 70% of the elastic limit stress for a UHPFRC subjected to the elastic domain, at about 55–65% of the elastic limit stress for a UHPFRC subjected to the strain-hardening domain, and 45% in the strain-softening domain.

2.2. Methodology

To determine the failure mechanism of short threaded anchors embedded in the UHPFRC and their pull-out resistance, a numerical approach was found to be efficient. The tensile and compressive properties of the UHPFRC had already been tested through many uniaxial tensile and bending tests [4,5]. These tests were used to calibrate the simulated material properties for the numerical model, which was subjected to a continuously increasing uniaxial pull-out force.

The numerical analysis was conducted using the finite element software ATENA [6]. The suitability of this program for the intended purpose was confirmed by the first author's prior experience in investigating the damage of load-bearing structures made of reinforced concrete, including the Gotschna road tunnel and the Adler railway tunnel in Switzerland. Additionally, ATENA was used for designing rehabilitation measures for the fixed railway track at Zurich Airport station using UHPFRCs [1]. In the damage investigations of the mentioned tunnels, monitoring was conducted, which validated the results of the numerical analysis.

In the frame of this research, the numerical modeling was carried out as follows:

1. The simulation of previously conducted 4-point bending tests, following [4] (pp. 53–54), using UHPFRC properties from test B4 (p. 62): the numerical model was also tested using UHPFRC properties of specimen T1-2 from [4] (p. 34 Table 3, p. 30) and specimen TIII 000-1 from [5] (p. 19 Table 3.2, p. 94); the simulated 4-point bending test served as an auxiliary model;
2. The calibration of the finite element mesh using the auxiliary model;
3. The simulation of the numerical model to investigate pull-out resistance;
4. Sensitivity analysis and the calibration of the finite element mesh size.

The geometry of the steel anchor was slightly modified for numerical purposes; the flanks of the threaded anchor were modeled with the same surface, thread angle, and pitch as a B500B rebar with a diameter of 20 mm, but without a helix angle. Thereby, the 5 mm width flanks were modeled to ensure the force introduction over the contact surfaces between the UHPFRC and threaded anchor according to Figure 3.

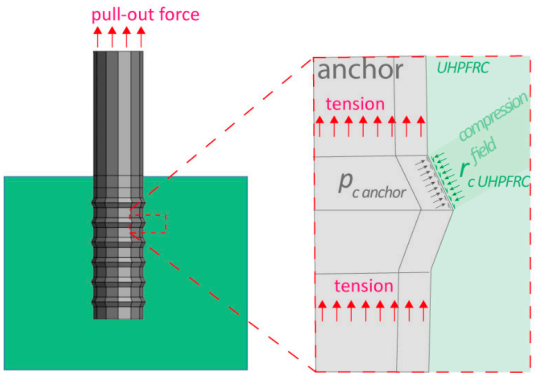


Figure 3. Stress transfer from steel anchor to the UHPFRC along the contact surface of the anchor rib with the UHPFRC.

3. Literature Review

Previous laboratory tests were mainly conducted on fiber-reinforced concretes, high-performance fiber-reinforced concretes, or different types of UHPFRCs with low steel fiber content, usually 0.1–1.6%. In addition, epoxy glue and other synthetic materials were used as bonding materials for the anchors. In some cases, the UHPFRC itself was used as a bonding material for the post-installed anchors in concrete [7]. All reported laboratory tests failed via anchor pull out (Figure 1c), fracture of the anchor (Figure 1b), or a combined fracture (Figure 1d), except the particular type of facade anchors discussed below. Thus, the pull-out resistance of the UHPFRC could not be directly determined, nor could the structural behavior be investigated based on these laboratory tests.

Satoh et al. [7] conducted pull-out tests on post-installed adhesive anchors in concrete, which were fixed in a borehole of 30 mm diameter using a UHPFRC, and analyzed the results using a finite element model. The anchors with 25 mm, 50 mm, and 75 mm embedment lengths were tested. The UHPFRC, with a compressive strength of 100 MPa and tensile strength of 10 MPa, had a fiber content of only 1.57 vol. %. The tests revealed that the pull out of a concrete cone (similar to Figure 1a) occurs in the case of the shortest anchor with an embedment length of 25 mm, and the combined fracture mode was observed in the case of 50 mm and 75 mm embedment lengths (Figure 1d). This research showed that using a UHPFRC instead of the grouting mortar increases the bond between anchor and concrete and thus increases the pull-out resistance of anchors fixed in concrete. In addition, the finite element analysis [7] showed that critical cracks appeared in concrete and led to the formation of the fracture cone.

Kalthoff et al. [8] investigated the pull-out behavior of threaded anchors with a relatively short pitch in UHPC (ultra-high-performance concrete) with 0.62% to 1.86% fiber content and traditional concrete. The pull-out resistance in the tested UHPC was up to 53% higher than in the traditional concrete. Moreover, it was pointed out that using short anchors in concrete is unreliable and, thus, not recommended. A good bond was achieved only in the case of anchorage in UHPC. Furthermore, the same fracture mechanism for UHPC and traditional concrete was initially assumed. However, no specific investigation of the fracture mode was conducted, and thus, the results could not be used for the interpretation of the fracture mechanisms observed in this work.

Fehling and Lorenz [9] investigated the bond behavior of rebars in UHPC. They performed three series of pull-out tests on rebars with the diameters d_s = 12 mm and 14 mm

anchored in UHPC with 0.1% to 1.5% steel fiber contents, in which different parameters were varied:

1. The first test series investigated the influence of UHPC cover thickness on the fracture mode. The pull-out force was applied to the rebars with embedment lengths ranging from 2 d_s to 12 d_s anchored in the UHPC specimens with a UHPC cover of 1 d_s to 2.5 d_s. It was found that the increase in UHPC cover leads to a disproportionately lower increase in the average bond strength at maximum force. Furthermore, the splitting of UHPC was observed in the case of rebars with an embedment length of 8 d_s anchored in UHPC of 1% fiber content and UHPC cover smaller than 2.5 d_s.
2. The effect of conventional steel reinforcement bars deployed in the transverse direction was investigated in the second series. The pull-out force was applied to the rebars with an embedment length of 2 d_s to 5 d_s anchored in the specimens with a UHPC cover of 1 d_s to 2.5 d_s. The results show that transverse reinforcement bars do not increase the pull-out resistance in the tested case.
3. The influence of the fiber content on the bond strength was investigated in the third series, which was performed on the UHPC specimens with a length of 780 mm, width of 300 mm, and height of 360 mm with anchored rebars with embedment lengths of 3.5 d_s and 5 d_s. The steel fiber content was 0.5, 1, and 1.5%. The type of fiber and the heat treatment were the same as in the second test series. The UHPC cone fracture type was observed in the case of a UHPC cover larger than 2 d_s and embedment length of 3.5 d_s to 5 d_s. In the case of a very large (not exactly defined) UHPC cover, a combination of UHPC cone and splitting cracking was observed.

The tests reveal that UHPC with a fiber content up to 1.5% behaves similarly to traditional concrete. Thereby, the UHPC cone fracture in analogy to Figure 1a occurs just in the case of the shortest embedment length, which was of sufficient size to allow for fracture cone formation. Moreover, on the photo showing the fracture mode (Figure 7 in [9]), radial cracks are identified, which indicates that the tensile strength of UHPC in the tangential direction around the rebars was reached.

Grzesiak et al. [10] investigated facade anchors fixed in high-performance polypropylene fiber-reinforced concrete (HPFRC). The stiff polypropylene fibers with a diameter of 0.70 mm and a length of 30 mm are three times larger than typical steel microfibers (for instance, the steel microfibers in a commercially available UHPFRC mix are 13 mm long and have a diameter of 0.175 mm). Two types of facade anchors with embedment lengths of 25 and 26 mm were used. In both cases, the fracture mode was a pulled-out HPFRC cone, which is very similar to the typical fracture cone in concrete, according to Figure 1a. Thereby, the inclination between the fracture surface and the specimen surface was about 35°. In the case of the adjustable suspended tension anchor, the pull-out resistance of the HPFRC cone increased up to 250% with increasing polypropylene fiber content from 10 to 35 kg/m^3. The pull-out tests for the adjustable spacer bolt showed no significant improvement in the pull-out resistance due to increased fiber content.

Vita et al. [11] investigated the behavior of bonded anchors with diameters of 16 and 24 mm in steel fiber-reinforced concrete (SFRC) with embedment lengths between 50 and 125 mm under tensile loading. The research revealed that in an SFRC with fiber content between 20 and 80 kg/m^3, the decisive failure mode is the pull out of a concrete cone, as shown in Figure 1a.

The research findings indicate that increasing the steel microfiber content increases the pull-out resistance [12–15]. Generally, a better bond can be achieved between a threaded steel anchor and a UHPFRC than in concrete [16]. With increasing steel microfiber content, the fracture mechanism changes from a pure fracture cone, according to Figure 1a, to a combined fracture mechanism, according to Figure 1d. Furthermore, in a UHPFRC with polypropylene fibers, just as in a steel fiber-reinforced concrete, an increase in the pull-out resistance of the fracture cone is observed. The fibers that traverse the fracture surface are anchored on both faces of the crack, transmitting tensile stress.

4. Numerical Simulation

4.1. Aim

Current non-linear FE programs allow for accurate modeling of the properties of cementitious building materials and structural elements to simulate the structural behavior up to maximum resistance and into the post-peak domain. These FE models are often used for detailed analysis of laboratory test results and investigations of the mechanical behavior of structures, considering specific loading conditions. Such finite element simulations presuppose that the cementitious building material is idealized as a continuum with a predefined constitutive stress–strain law.

In the following section, the structural behavior of a UHPFRC near a short threaded anchor subjected to uniaxial quasi-static loading is investigated by means of non-linear finite element analyses. Moreover, it will be demonstrated that numerical simulation is an efficient approach for designing laboratory tests or for in situ monitoring of structures.

4.2. Numerical Model

The presented numerical model corresponds to a common and frequently encountered application scenario for increasing the load-bearing capacity of a reinforced concrete (RC) slab due to the application of a UHPFRC layer and the need to fix a tensile element on the top of a slab. To the existing RC element, a 50 mm thin layer of a UHPFRC is added. An alternative application case to the building of the numerical model could also be a model that represents a thin UHPFRC structural part, but, in this case, an additional boundary condition would be needed to obtain compliance of this thin structural part under the pull-out force, for instance, fixing a thin UHPFRC structural part along the surface in order to avoid the deformation in the force direction [17,18].

Furthermore, as known from numerous laboratory tests and realized projects, a monolithic bond is obtained between the concrete and the UHPFRC layer. Thus, the numerical model assumes a monolithic bond between both building materials and that no cracking or fracture occurs in the concrete layer below the anchor. Based on this, assigning only UHPFRC properties to the macro-elements representing the UHPFRC part of the composite slab is sufficient, making the numerical analysis easier and more efficient. Figure 4a presents the concept of the numerical model. A rectangular element ① of 0.5 m × 0.5 m × 0.5 m is cut from a large composite slab, consisting of a concrete part with a thickness of 0.45 m and a UHPFRC layer of 50 mm, which are monolithically connected. A short threaded anchor of 20 mm diameter ②, with an embedment length of 50 mm and six force-transmitting flanks, is fixed in the UHPFRC layer during casting. The size of the anchor flank surface corresponds to a common rebar. Figure 4b shows the numerical model using the finite element program ATENA [6]. The anchor is modeled with six 5 mm wide flanks distributed evenly along the embedded part according to Figure 3. Because of the non-orthogonal shape, a tetrahedral mesh with an element size of 3 mm was assigned to the anchor. The simulated slab part is subdivided into three areas. The inner orthogonal macro-element around the anchor with a size of 0.1 m × 0.1 m × 0.1 m (Figure 4b) has the same mesh type and size as the anchor. The macro-element anchor and the macro-element UHPFRC are monolithically connected to simulate the UHPFRC–steel bond behavior. The outer upper area of the UHPFRC element is subdivided into eight orthogonal macro-elements, to which the hexahedral mesh type with an element size of 23 mm was assigned. The lower area of the UHPFRC element serves only for self-weight and is statically irrelevant, as only the upper area will be affected, as shown below. This area was subdivided into nine orthogonal macro-elements with hexahedral mesh of a 100 mm element size for geometrical reasons. All macro-elements representing the UHPFRC are monolithically connected. The size of the finite elements in the numerical model was iteratively determined, calibrated using the auxiliary model according to Section 2.2, and tested to ensure force transmission from the anchor to the UHPFRC over the surfaces of the flanks.

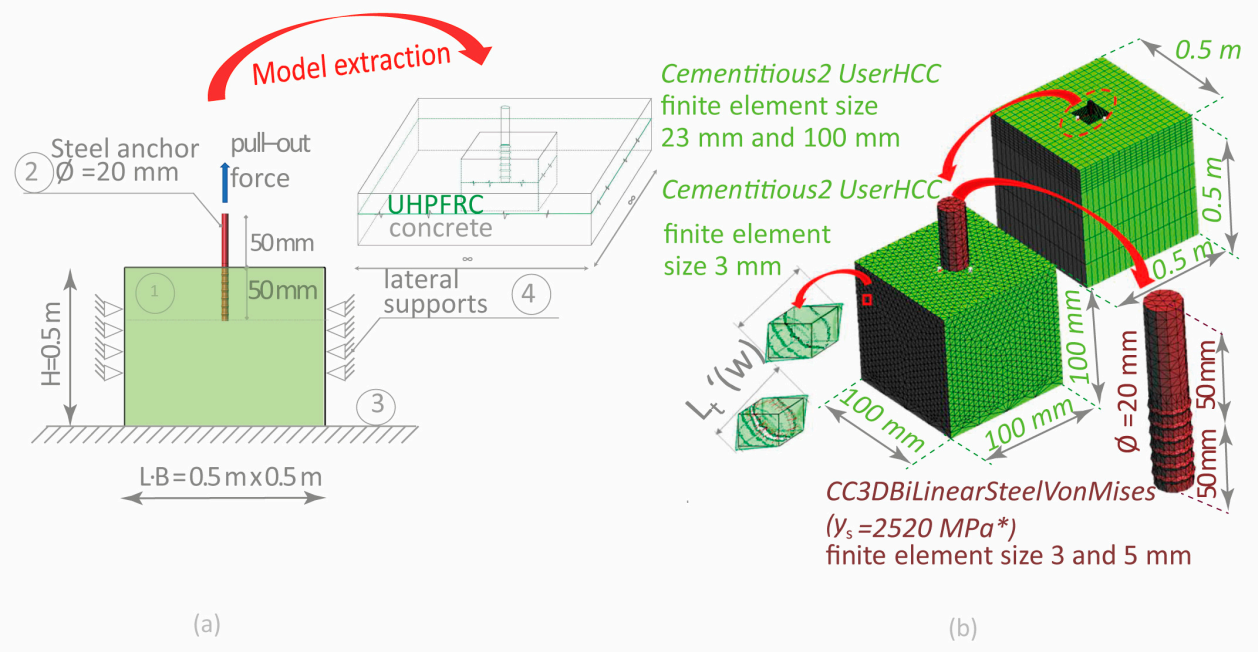


Figure 4. Numerical simulation: (**a**) schematic illustration of the set-up; (**b**) numerical model and illustration of the formation of discontinuities and the propagation of a fictitious crack in the finite element.

Note that the size of the representative slab part (Figure 4a) has been chosen so that the horizontal supports ④ are placed outside the area with the UHPFRC–anchor interaction. The self-weight of this representative slab part is greater than the maximum pull-out force, such that the reaction of the vertical support ③ is always in compression. In addition, since the focus is to analyze the structural behavior of the UHPFRC and how the pull-out force is introduced in the UHPFRC's structural parts, the numerical simulation of anchor slip in the UHPFRC is not performed, since the term slip refers to the limited abrupt displacement of the anchor, during which no force is introduced into the UHPFRC. A sensitivity analysis was performed to justify this assumption. For this, the interface elements between the anchor and the UHPFRC macro-elements were inserted into the original model, and the horizontal stiffness was varied. This sensitivity analysis showed that no slip was observed even at very low horizontal stiffness in the case of this specific numerical model, and as a result, the compressive force introduced in the UHPFRC above the anchor flanks remains the same during each loading step in the numerical models with and without interfaces. The only obvious difference between both models was the computing time, which was longer in the case of the model with interfaces. This sensitivity analysis does, however, not claim that a slip between the UHPFRC and the anchor could not occur in real structural elements.

Furthermore, Figure 3 shows the concept of force introduction from the threaded anchor into the UHPFRC bulk material, as considered in the numerical model. The applied pull-out force causes tensile stress in the anchor, which leads to compressive stress acting on the contact surfaces between the anchor flanks and the UHPFRC. The resulting inclined upward compressive stress fields in the UHPFRC lead to the formation of a horizontal near-surface tensile stress field in the UHPFRC, as will be discussed below. The maximum compressive force that can be introduced into the UHPFRC over a flank is limited by the compressive strength of the UHPFRC.

4.3. Modeling of UHPFRC

The theoretical background of the numerical modeling of the UHPFRC and the programming aspects are described in detail in [19]. The following is a summary of the relevant steps of numerical computation in ATENA: Table 1 summarizes the mechanical properties of two UHPFRC products used in this study. Both commercially available UHPFRC products were already used in previous research for laboratory tests. UHPFRC 7 corresponds to

TIII 000-1 according to [5] (p. 94), and UHPFRC 11 corresponds to T1-2 according to [4] (p. 30). The materials used, UHPFRC7 and UHPFRC11, are fine-grained cementitious fiber-reinforced composite materials with a maximum grain size of 0.5 mm, which are considered as a homogeneous, isotropic bulk material in this particular case.

Table 1. Tensile properties of the two used UHPFRC products.

Tensile Properties of UHPFRC According to [4] (p. 34 Table 3, p. 30) and [5] (p. 19 Table 3.2, p. 94)			**UHPFRC11**	**UHPFRC7**
Tensile strength	f_{UItu}	[MPa]	11.5	7.1
Elastic limit	f_{UIte}	[MPa]	9.8	6.9
Strain in the UHPFRC at the tensile strength	ε_{Utu}	[‰]	2.29	1.5
Strain in the UHPFRC at the elastic tensile strength	ε_{Ute}	[‰]	0.22	0.15
Fiber length	l_f	[mm]	13	13
Fiber diameter	d_f	[mm]	0.175	0.16
Fiber content	Vol.	[%]	3.8	3.0

The mechanical properties of UHPFRC were modeled using a fracture-plastic material model (CC3DNonLinCementitious2User [19], in which the constitutive models for tensile and compressive behavior are combined. The fracture model is based on the smeared crack model that presupposes the Rankine failure criterion. A pointwise defined tensile softening law close to a linear function is used (Figure 5). The plasticity model is based on the Menétrey-Willam failure surface. The fracture and plasticity models are combined by the strain decomposition method after De Borst [20] and the return mapping algorithm is used to determine the elastic predictor. Due to strain decomposition after De Borst [20] into elastic $\varepsilon_{ij}{}^{e}$, plastic $\varepsilon_{ij}{}^{p}$, and fracture $\varepsilon_{ij}{}^{f}$ components ($\varepsilon_{ij} = \varepsilon_{ij}{}^{e} + \varepsilon_{ij}{}^{p} + \varepsilon_{ij}{}^{f}$, $i,j = 1, 2, 3, 4$), the stress equivalence in both models is guaranteed. The new stress state is determined according to the formula $\sigma_{ij}{}^{n} = \sigma_{ij}{}^{n-1} + E_{ijkl}(\Delta\varepsilon_{k} - \Delta\varepsilon_{kl}{}^{p} - \Delta\varepsilon_{kl}{}^{f})$, where the $\Delta\varepsilon_{kl}{}^{p}$ and $\Delta\varepsilon_{kl}{}^{f}$ are increments of plastic and fracture strain. As mentioned above, the Rankine criterion $F_i{}^{f} = \sigma_{ij}{}^{t} - f_{ti} \leq 0$ is considered in the numerical simulation of the softening behavior [19], where $\sigma_{ij}{}^{t}$ is the tensile stress calculated according to the formula: $\sigma_{ij}{}^{t} = \sigma_{ij}{}^{n-1} + E_{ijkl}(\Delta_{\varepsilon kl}{}^{e\,calc} + \Delta_{\varepsilon kl}{}^{p\,calc} + \Delta_{\varepsilon kl}{}^{f\,calc})$, f_{ti} is the tensile strength in the principal stress direction i, and k is the failure surface. If the calculated tensile stress $\sigma_{ii}{}^{t}$ is higher than the tensile strength f_{ti}, then, in the next iteration step n, the tensile stress is recalculated such that the final tensile stress satisfies the condition: $F_i{}^{f} = \sigma_{ii}{}^{n} - f_{ti} = 0$.

Assuming that the increment of fracture strain $\Delta_{\varepsilon kl}{}^{f}$ is normal to the failure surface k, it follows that $\Delta_{\varepsilon kl}{}^{f} = \Delta\lambda \cdot \partial F_k{}^{f}/\partial\sigma_{ij} = \Delta\lambda \cdot \delta_{ik}$, where $\Delta\lambda$ is the increment of the fracturing multiplier. By the substitution of the tensile stress $\sigma_{ii}{}^{n} = \sigma_{ij}{}^{t} - E_{ijkl} \cdot \Delta_{\varepsilon kl}{}^{f}$ and the increment of the fracture strain $\Delta\varepsilon_{kl}{}^{f}$ into $F_i{}^{f} = \sigma_{ij}{}^{t} - f_{ti} = 0$, the fracturing multiplier is determined as follows: $\Delta\lambda = \sigma_{kk}{}^{t} - f_{tk}/E_{kkkk}$. Furthermore, the crack opening $w_k{}^{max}$ is determined by the sum of the total value of the fracture strain $\varepsilon_{kk}{}^{f}$ and the current increment of the fracturing strain $\Delta_{\varepsilon kk}{}^{f} = \Delta\lambda \cdot \delta_{kk}$, multiplied by the characteristic length L_t: $w_k{}^{max} = L_t(\varepsilon_{kk}{}^{f} + \Delta\varepsilon_{kk}{}^{f})$. It should be noted that, in the present study, the characteristic length L_t is defined as the projection of the geometric size of the finite element on the axis in the direction of the principal strain and corresponds to the characteristic crack (The definition of "crack" in the case of UHPFRC means multiple fine cracking of the cementitious matrix of UHPFRC. Tensile stress is transmitted by the steel fibres. In this paper, this type of cracking is called "matrix discontinuity") bandwidth [21], as shown in Figure 4b.

Furthermore, Figure 5 presents the tensile law of UHPFRC, modeled pointwise in the elastic, strain-hardening, and strain-softening domains. Until the localization of strain (ε_{tloc}), the stress–strain curve corresponds to the stress–strain constitutive law. After exceeding the localized strain ε_{tloc}, the material law is adjusted to the actual crack band L_t [22] as follows: $\varepsilon^{f}{}_{l\,current} = \varepsilon^{t}{}_{loc} + (\varepsilon^{f}{}_{l} - \varepsilon^{t}{}_{loc})/L_t/L^{t}{}_{ch}$, thereby, $L^{t}{}_{ch}$ is the measuring base used to determine the strain value.

Note that the mentioned crack band model was initially developed for concrete. Since concrete is a cementitious material with low tensile strength and without a strain-

hardening domain, tensile strain softening occurs immediately after reaching the tensile strength when the fictitious crack starts to develop. Unlike concrete, UHPFRC shows matrix discontinuities and no real crack until reaching the deformation w ($\varepsilon^f_l = l_f/2$) corresponding to half of the maximum fiber length l_f. Therefore, the crack band model can be interpreted as a discontinuity band model in the case of UHPFRC.

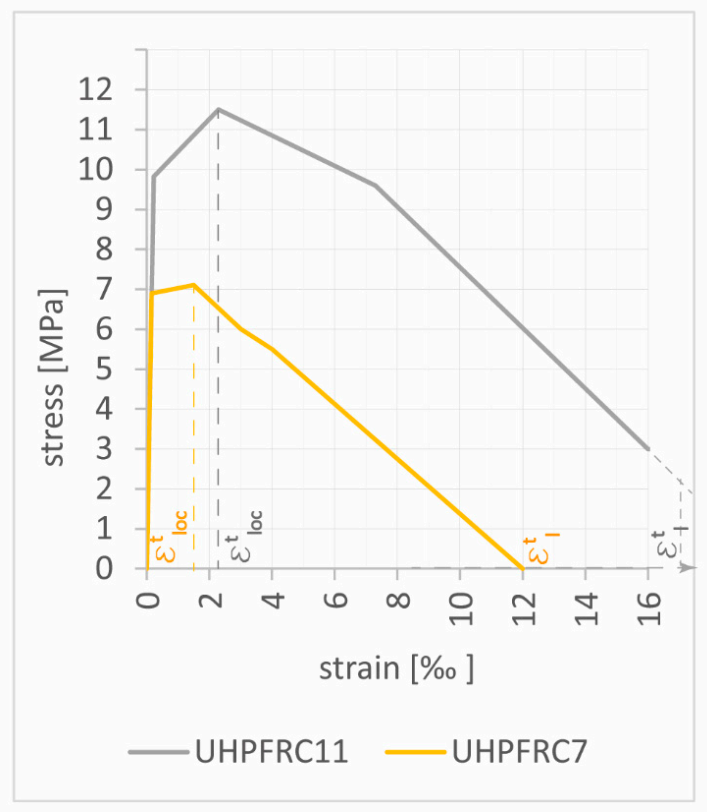


Figure 5. Assumed tensile stress–strain curves based on the tensile properties of the two UHPFRC products according to Table 1.

5. Numerical Simulation of the Quasi-Static Structural Behavior of the UHPFRC Substrate

Modeling of Quasi-Static Loading

The quasi-static pull-out force is modeled as a gradually increasing uniaxial force with 5kN per loading step acting at the top of the steel anchor. To simulate the post-peak domain, the arc-length solution method was used [19]. Note that for studying this model, knowing the exact force introduced into the UHPFRC body is crucial. Therefore, the introduced force in the UHPFRC body is monitored on the level of the top UHPFRC surface, as shown in Figure 6. This modeling results in the pull-out force–displacement curves shown in Figure 7. The finite element simulation ran until no more change in the introduced pull-out force was observed in the post-peak domain (Supplementary Materials). The numerical simulation was interrupted manually when at a constant pull-out force the displacement at point *O* (Figure 6) was increasing, which was interpreted as pulling out of the threaded steel bar from the UHPFRC substrate.

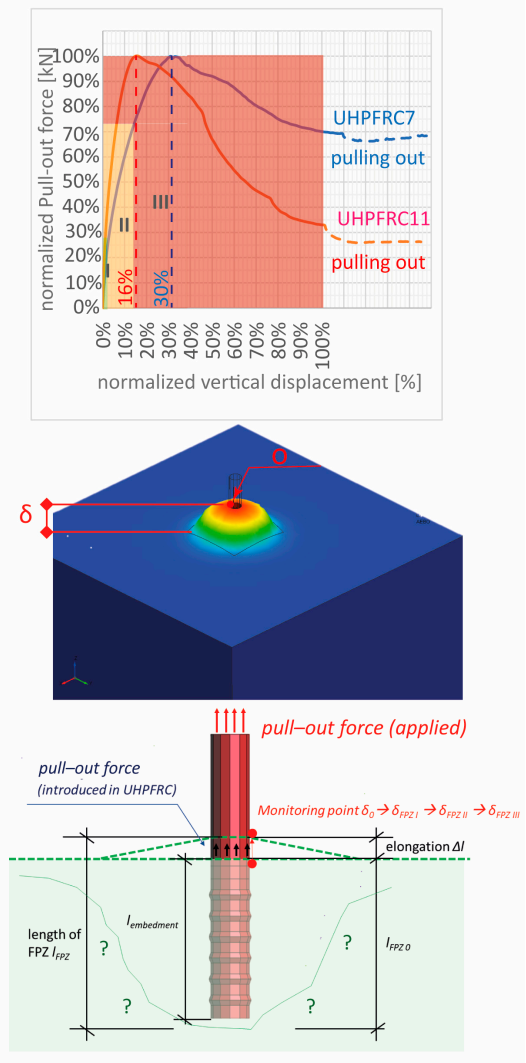


Figure 6. Normalized pull-out force–displacement diagrams for pulling the threaded anchor Ø 20 mm $l_{embedment}$ = 50 mm out of two different UHPFRC types.

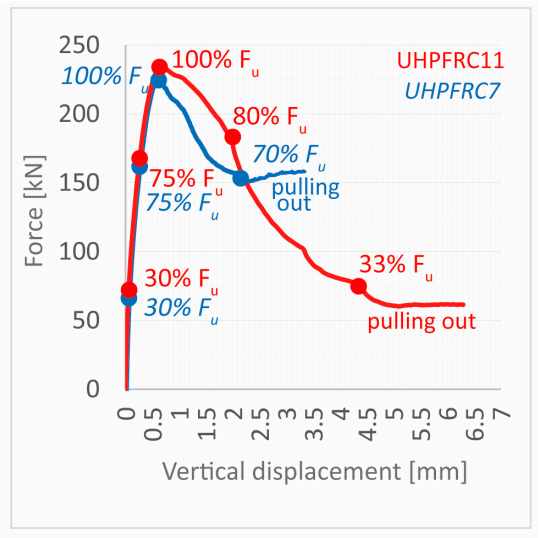


Figure 7. Force–displacement diagram for UHPFRC7 and UHPFRC11.

6. Results

6.1. Pull-Out Force–Displacement Curves

To investigate the effect of increasing the tensile strength of the UHPFRC on the force–displacement behavior and the fracture mode, the force–displacement diagram was normalized. Figure 6 presents the normalized pull-out force–displacement curves obtained for UHPFRC11 and UHPFRC7. Thereby, the maximum vertical displacement is assumed to be the displacement at which no more force change was registered; respectively, the threaded anchor will be pulled out from the UHPFRC substrate. It can be seen that the ultimate force F_u of the anchorage was achieved at 16% of the maximum vertical displacement for UHPFRC11 and 30% of the maximum displacement for UHPFRC7.

The analysis of the absolute magnitudes of force and displacement (Figure 7) reveals that the computed ultimate force of the anchorage is similar, i.e., 234 kN in UHPFRC11 and 227 kN in UHPFRC7, being reached at the same vertical displacement of 0.7 mm in both cases. However, the post-peak domain is different. In UHPFRC7, the post-peak domain shows relatively little deformation, while the force decreases to 70% F_u with increasing vertical deformation thereafter at constant force, indicating a pulling-out mechanism. In the post-peak domain of UHPFRC11, the force decreases to 33% F_u, then only the vertical deformation near the anchor increases.

In both cases, no real crack occurs in the tensile membrane during the entire loading process. The strain increase in the membrane leads to a widening of the opening between the UHPFRC and the anchor. This means that the ultimate force of the anchorage does not correspond to the ultimate resistance of the UHPFRC membrane. Moreover, the numerically simulated pull-out behavior shows three domains with different slopes, corresponding to three stages of the pull-out process. Therefore, for the detailed analysis of the numerical results, the entire loading process is subdivided into three phases: Phase I: loading up to 30% F_u, Phase II: loading up to 75% F_u, and Phase III: loading up to 100% F_u and post-peak. Using plots of principal strains at each loading phase and in the post-peak domain, the tension and compression fields and, thus, the fracture process are analyzed as follows:

6.2. Pull-Out and Fracture Processes

Figure 8a,b show plots of maximum principal strain at the end of phases I, II, and when achieving 100%Fu [18]. These plots are supplemented with red and blue arrows to clarify the development of tension and compression fields. The red arrows highlight the tensile strain propagation in the radial direction, and the blue arrows show the direction of the compression field extension extracted from the plots of minimum principal strain. Positive values of principal strains correspond to tension and negative values to compression.

In phase I, which extends from 0 kN to 30% F_u, the pull-out process starts to propagate in the upper part of the UHPFRC layer around the threaded anchor within an approximately 5 mm thin horizontal circular tension strain field (ε_{rad}). Additionally, an inclined tensile strain field (ε_{cone}) develops perpendicular to the UHPFRC cone forms.

These strain fields reveal that the pull-out force introduced via the threaded anchor produces initially conical compression ($-\varepsilon$) and circular horizontal tension fields (ε_{rad}) in the near-surface UHPFRC layer. If no fracture of the steel anchor occurs, and compression ($\sigma_{compession}(-\varepsilon) \leq f_{Uc}$) and tension ($\sigma_{tension}(\varepsilon_{rad}) \leq f_{Utu}$) are transmitted in the UHPFRC substrate, the anchorage is functional. Thereby, the UHPFRC next to the threaded anchor enters into the strain-softening domain, already at F = 10–15% F_u. The UHPFRC in the softening domain in the state at the end of phase I (30%F_u) is shown with an orange color for UHPFRC7 and a purple color for UHPFRC11 according to the scale on the right of Figure 8a,b. Furthermore, the inclined tensile strain field (ε_{cone}) extends over the entire UHPFRC region that comprises the threaded anchor and the UHPFRC cone, including the mentioned circular horizontal tensile (ε_{rad}) and conical compression ($-\varepsilon$) strain fields. In addition, phase I is characterized by the quasi-linear path on the force–displacement diagram, indicating elastic behavior.

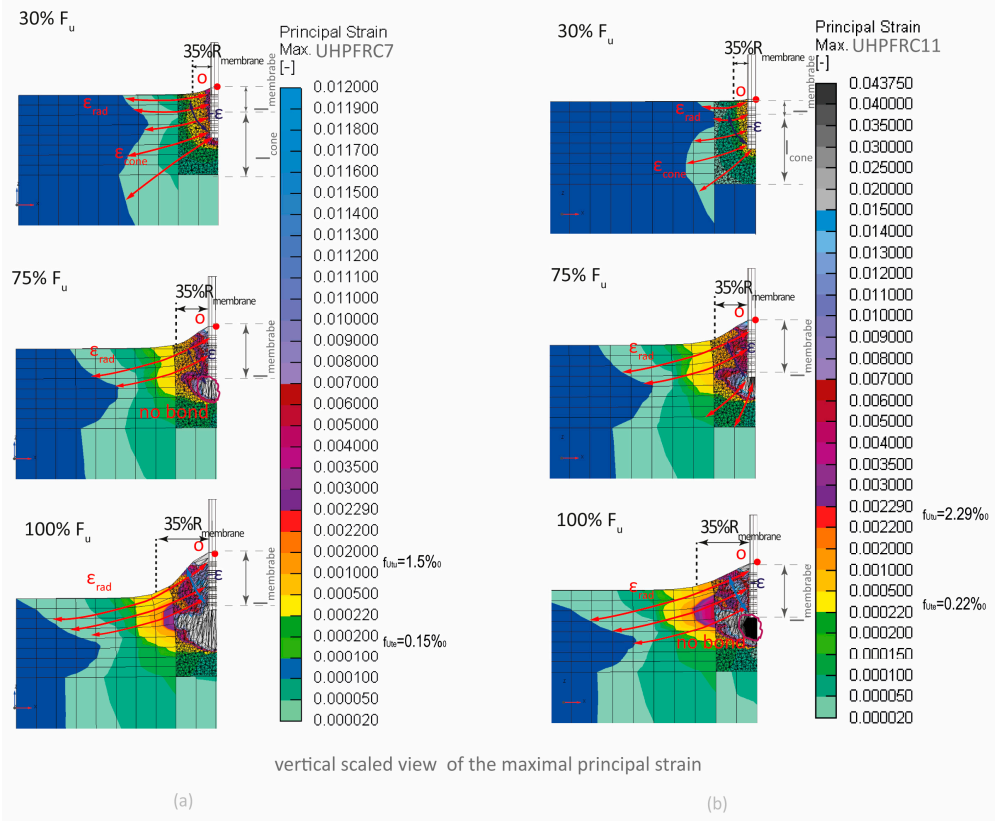


Figure 8. Monitoring the fracture process in UHPFCs using maximum principal strain plots: (**a**) development of the membrane in the UHPFRC7; (**b**) development of the membrane in the UHPFRC11.

During phase II, extending up to 75% F_u, the horizontal circular tensile strain field (ε_{rad}) increases further and encompasses the UHPFRC cone (l_{cone}) completely, as depicted by the plots of principal strains.

Moreover, with an increasing circular tension strain field (ε_{rad}, $l_{membrane}$), the height of the UHPFRC cone decreases ($l_{cone} \rightarrow 0$). And at the end of phase II, the anchorage mechanism consists of the circular tension field of thickness ($l_{membrane}$) alone, which is equal to the embedment length of the threaded anchor $l_{embedment}$. From a static viewpoint, the circular tension strain field (ε_{rad}) behaves like a tensile membrane. On the force–displacement diagram, phase II is characterized by non-linear force–displacement behavior between 30% F_u and 75% F_u.

Phase III begins with the fully formed tensile membrane of thickness $l_{membrane} \approx 1.0 - 1.1$ $l_{embedment}$ as the main resisting part against the pull-out force. Since the pull-out force acting through the threaded anchor leads to compression at the contact surfaces between the anchor flanks and the UHPFRC (Figure 3), the inclined conical compression strain field ($-\varepsilon$, Figure 8a,b) is also observed within the tensile membrane and causes additional increasing tensile strain in the upper third of the tensile membrane.

6.3. Failure Process Within the Tensile Membrane

Next, the failure process within the tensile membrane is analyzed. Figure 9 schematically presents the strain (ε_{rad}) and stress (f_t) distributions within the tensile membrane. Figures 10 and 11 show the state of the strain distribution in the radial direction (ε_{rad}) in the annular circular tensile membrane every 54 kN until F_u is reached. The step of 54 kN was chosen iteratively to monitor the development of the tensile membrane. The dashed arrows indicate the radius of the tensile membrane that corresponds to the loading given on the dashed arrows. According to the legend below the diagrams, the color curves present the strain distribution within the tensile membrane in the mentioned loading steps.

From these diagrams, the development of the tensile membrane and the strain distribution during the entire loading process can be depicted. The diagram shows that the maximum radius ($R_{membrane}$) is 250 mm, and the outer part of the membrane, corresponding to 60% of the membrane radius, remains in the elastic domain during the entire loading process. The UHPFRC next to the anchor enters into the softening domain, still within loading phase I according to Figure 8. The comparison of Figures 10 and 11 reveals that the tensile membrane in UHPFRC11 is bell shaped and more pronounced in the inner part than in UHPFRC7, whereas the tensile membrane in UHPFRC7 is less pronounced and shows the shape of an arch.

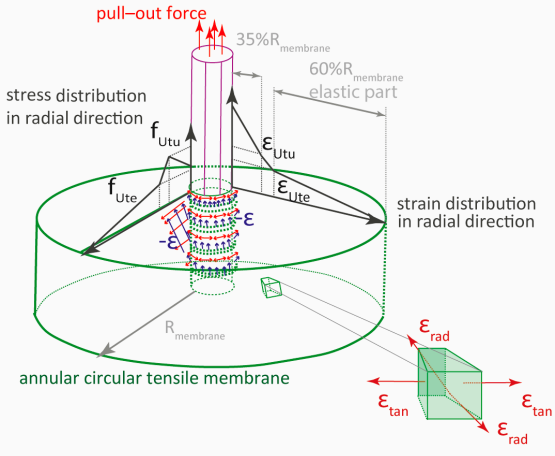


Figure 9. Schematic representation of the stress and strain distributions within the tensile membrane.

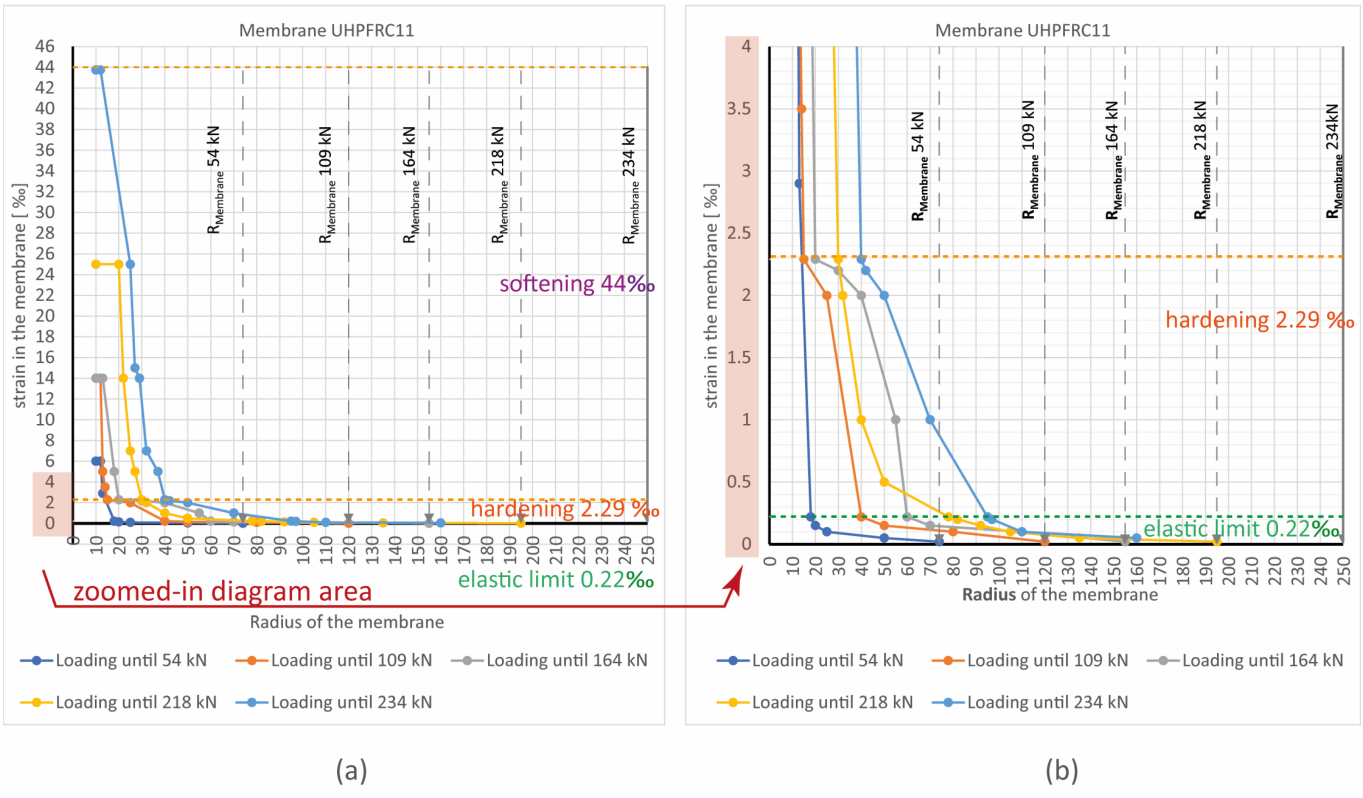


Figure 10. Strain distribution in the tensile membrane of UHPFRC11: (**a**) strain distribution in the entire membrane in the range of 0 to 44 per mille; (**b**) zoomed-in area that is between a strain distribution of 0 and 4 per mille.

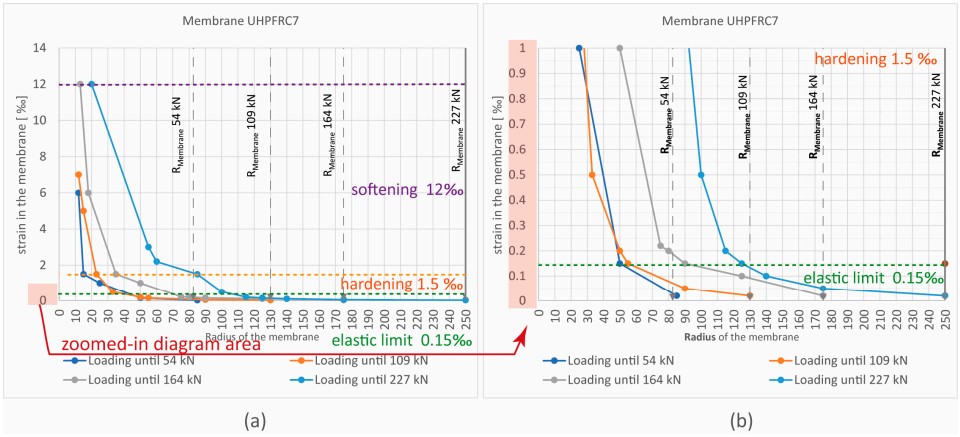


Figure 11. Strain distribution in the tensile membrane of UHPFRC7: (**a**) strain distribution in the entire membrane in the range of 0 to 14 per mille; (**b**) zoomed-in area that is between a strain distribution of 0 and 1 per mille.

Furthermore, the diagrams shown in Figure 12 provide the main parameters, i.e., the radius of the tensile membrane $R_{membrane}$ and the thickness of the membrane $l_{membrane}$ during the loading process. During loading phases I and II, the tensile membrane forms, and the rate of increase in the radial direction is up to five times higher than in the vertical direction.

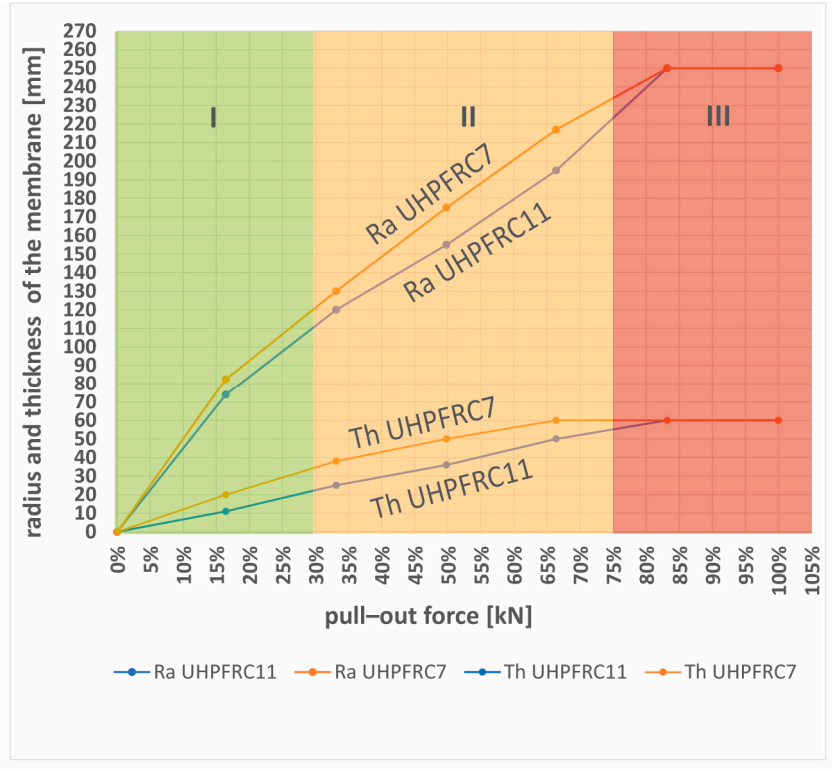


Figure 12. Radius (Ra) and thickness (Th) of the membrane, with increasing pull-out force.

The tensile stress remains constant within a limited part of the membrane, with a constant diameter where failure occurs. However, more volume is activated within the substrate around the anchor where the tensile membrane develops, and the tensile stress is distributed such that the outer part of the tensile membrane, corresponding to 60% of the radius, remains elastic. Thus, the membrane maintains force balance during the entire loading process.

6.4. Effect of the Tensile Membrane

The principal instrument employed in this research is numerical simulation, which allows for an investigation of the distribution of tensile and compressive stress fields in a fine-grained cementitious material. Following our observation of the development of the tensile stress field in the upper area of the UHPFRC around the threaded anchor, which represents the main resistance against pull out, a sensitivity analysis was conducted. This involved reducing the tensile strength of the substrate material UHPFRC to 4 MPa, increasing it to 16 MPa, and replacing it with concrete, which has a tensile strength of 2.3 MPa and a compressive strength of 25.5 MPa (Figure 13a).

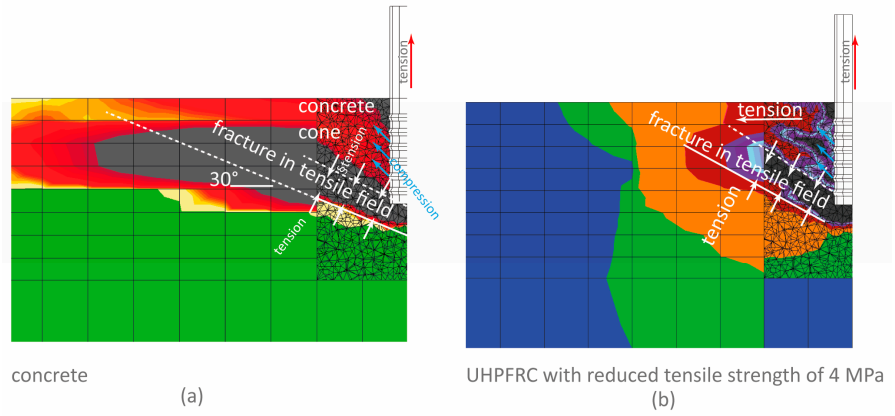


Figure 13. Monitoring the fracture process in the UHPFC using maximum principal strain plots: (**a**) pulling out of concrete cone; (**b**) fracture process in the UHPFRC with reduced tensile strength.

The sensitivity analysis demonstrated that an annular tensile stress field begins to form in a UHPFRC with a reduced tensile strength of 4 MPa (Figure 13b). But the formation of this tensile field takes place in the UHPFRC just close to the threaded anchor. The propagation of this tensile field in the horizontal direction already stops after the initial loading steps, since the UHPFRC reaches the softening domain in this limited area. The formation of the inclined tensile field perpendicular to the conical compression field became predominant, since this tensile field is larger, and the magnate of tensile stress increases more slowly. The fracture, respectively, the pull out of the so-called fracture cone, occurs due to reaching the tensile strength in this inclined tensile field in analogy to Figure 1a. The failure cone's inclination angle to the horizontal surface is approximately 30°. An analogous failure mechanism is also observed in the concrete with a tensile strength of 2.3 MPa (Figure 13a).

Increasing the tensile strength of the UHPFRC up to 16 MPa showed that the annular tensile field around the threaded anchor, which is called, in the frame of this research, the tensile membrane, propagates similarly to UHPFRC7 and UHPFRC11; thereby, the shape of the tensile membrane is more pronounced and bell shaped than in the case of UHPFRC11.

It should be noted that the reliability of the numerical model is no longer guaranteed for concrete with a grain size greater than 8 mm and an anchor embedment depth of 50 mm. For the numerical simulation, the substrate material UHPFRC was assumed to be an ideally homogeneous building material with strain-hardening and strain-softening behaviors, which, in the case of coarse-grained concrete with respect to the short anchor embedment length and width of anchor flanks, is no longer valid.

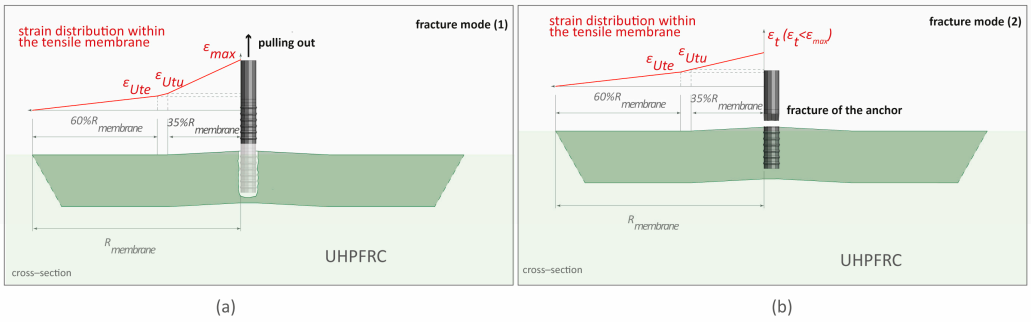
In addition, the fiber-reinforced concrete (FRC), according to [11], was not investigated in the frame of this research because fiber-reinforced concrete (FRC) shows fundamentally different mechanical properties and behaviors compared to UHPFRCs. FRC shows relatively low fiber content (max. 80 kg/m^3), and more than 30 mm long hooked fibers are integrated in the concrete with a maximum aggregate size up to 32 mm. Thus, FRC has a fundamentally different composition.

6.5. Features of the Failure Mode

This study principally aims to investigate the structural behavior of the anchorage of common threaded steel bars in UHPFRCs with given tensile properties as subjected to pull-out force using finite element analysis. The investigation of the structural behavior of UHPFRCs was possible because the numerical modeling allows us to assign sufficiently high tensile strength to the steel to avoid anchor fracture such that the failure mechanism in the UHPFRC becomes the determinant failure mechanism of the system.

The numerical simulations show that the introduction of a pull-out force in the UHPFRC body via a short threaded anchor leads to the formation of a tensile membrane in the near-surface UHPFRC with a thickness 1-1,1 $l_{embedment}$. The outer part of this tensile membrane, which corresponds to about 60% of the membrane radius, remains in the elastic domain during the entire pull-out process, while the thickness and radius of the tensile membrane increase. Thus, the fracture process zone is localized in the inner part of the annular circular tensile membrane of the UHPFRC, corresponding to about 35% of the membrane radius. In the radial direction, the tensile membrane develops up to five times faster than the thickness in the vertical direction. At about 85% of the ultimate force F_u, the tensile membrane is completely formed, with the thickness corresponding to the anchor embedment length $l_{embedment}$ and radius of about 5 $l_{embedment}$. The stress transfer in the completely formed tensile membrane occurs further via compressive stresses acting on the contact surface between anchor flanks and the UHPFRC, forming compression stress fields and increasing tensile stresses in the upper third of the tensile membrane. Finally, anchorage failure occurs due to the widening of the inner part of the annular circular UHPFRC tensile membrane around the anchor and, as a result, pulling out the anchor from the UHPFRC substrate. Thereby, no real cracks occur.

In summary, this study has revealed that the pull-out behavior of threaded anchors in a UHPFRC substrate fundamentally differs from the well-known pull-out behavior in concrete, according to Figure 1. For short threaded anchors in UHPFRCs, only two fracture modes are possible: (1) $F_{u,anchor} > F_{u,membrane}$: pulling out of the threaded anchor from the UHPFRC substrate (fracture mode (1), Figure 14a) or (2) $F_{u,anchor} < F_{u,membrane}$: fracture of the anchor (fracture mode (2), Figure 14b) [18].



(a) (b)

Figure 14. Failure modes of the threaded anchors in UHPFRCs: (**a**) fracture mode (1) when $F_{u,anchor} > F_{u,membrane}$; (**b**) fracture mode (2) when $F_{u,anchor} < F_{u,membrane}$.

Another feature of the structural behavior of the anchorage system is the plastic deformation in terms of failure indication:

- In the case of the tensile resistance of the anchor being lower than the pull-out resistance of the UHPFRC substrate ($F_{u,anchor} < F_{u,membrane}$), the plastic deformation of the threaded anchor would occur. This is the relevant case for the design of anchors in structural applications in engineering practice.
- In the case of the tensile resistance of the anchor being higher than the pull-out resistance of the UHPFRC substrate ($F_{u,anchor} > F_{u,membrane}$), the tensile membrane deforms within the inner 35% of the tensile membrane radius $R_{membrane}$ around the anchor. Comparing the vertical deformations in UHPFRC11 and UHPFRC7 at the

instant of anchorage failure, the vertical deformation of the annular circular tensile membrane with higher tensile properties was found to be more pronounced and localized around the threaded anchor. However, the vertical deformations remain very small compared to the fracture deformation of the anchor in steel. These vertical deformations are only 2 mm for UHPFRC7 and 4.5 mm for UHPFRC11. However, this failure mode can only occur if the threaded anchor with a diameter of 20 mm is made of high-strength steel (f_t > 700 MPa).

6.6. Anchor Steel

Since this study focuses on the investigation of fracture processes in UHPFRCs using finite element analysis, the steel tensile properties assigned to the anchor were assumed to be sufficiently high to avoid fractures in the anchor steel and to ensure force introduction into the UHPFRC substrate. Therefore, the tensile strength was assumed to be 2520 MPa (Figure 4b) after several trial simulations during the calibration of the numerical models. As shown in Figure 15, the maximum tensile stress in the anchor was 725 MPa. It follows that if a B500B rebar is used, the fracture would occur in the anchor ($f_t \approx 550$ MPa), so in order to introduce a force into the UHPFRC that will cause failure in the UHPFRC, a high-strength steel should be used as stated in 6.5.

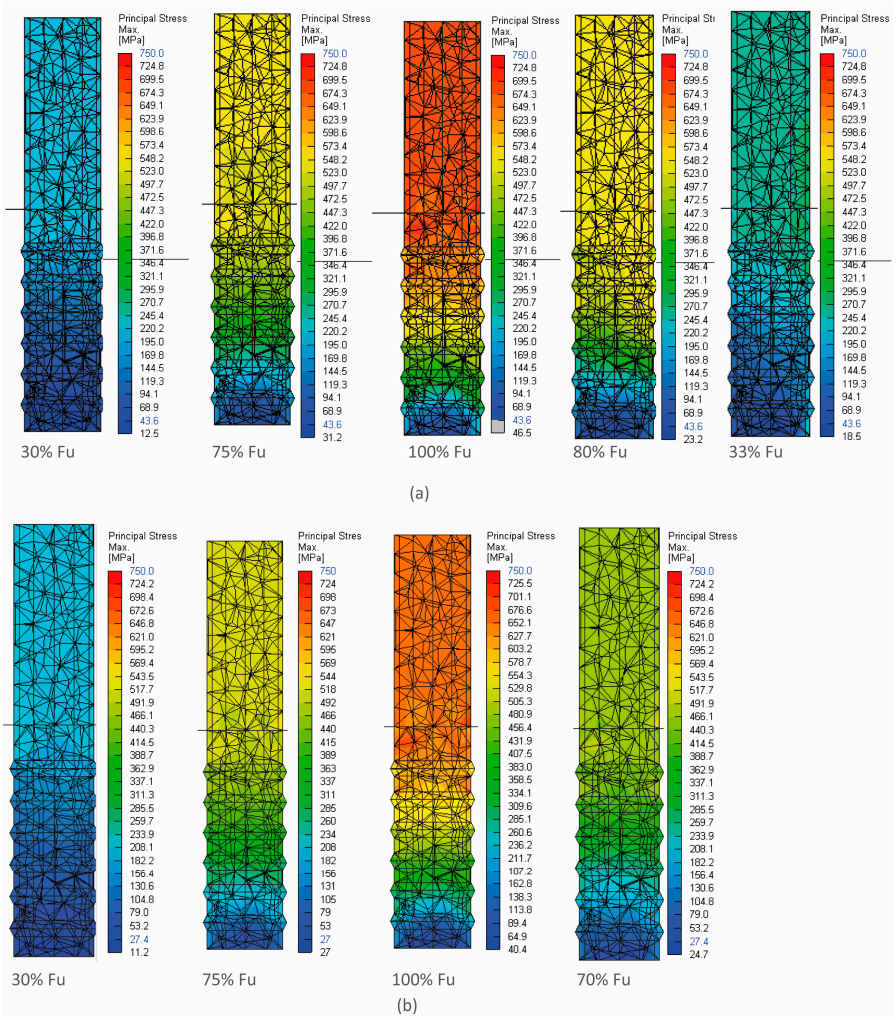


Figure 15. Maximum principal strain plots in anchor steel: (**a**) max. principal stress in threaded anchor in UHPFRC11; (**b**) max. principal stress in threaded anchor in UHPFRC7.

7. Limitation of the Research

In this research, only the pull-out resistance under quasi-static pull-out force was presented using numerical simulation. The authors also investigated the pull-out fatigue resistance under the uniaxial cyclic pull-out force. A direct approach using the finite element software ATENA was not applicable, since a numerical material model with strain-hardening features and an inclined unloading and reloading stress–strain curve was not available for the simulation of cyclic loading. In order to gain insights into how a cementitious material with the same tensile strength but without a strain-hardening domain behaves, numerical simulations were performed, in which the formation of the tensile membrane was again observed.

However, a theoretical approach for determining the fatigue resistance can be applied to estimate the fatigue resistance of the tensile membrane. A tensile membrane can be assumed to be a tension member with the fatigue endurance limit at a maximum fatigue level stress at about 45% of the elastic limit stress in the strain-softening domain.

8. Conclusions

1. This study shows that FE modeling is an efficient approach to discover possible failure mechanisms before laboratory tests are designed to focus on the research-relevant case. FE modeling allows us to vary building material properties, such as avoiding failure modes that are not research relevant, i.e., the fracture of the steel anchor.
2. Due to the UHPFRC's relatively high tensile strength and tensile deformation capacity, significant tensile stress fields form a tensile membrane in the UHPFRC substrate near the anchor when subjected to increasing quasi-static pull-out force.
3. With sufficient substrate size (i.e., the distance from the anchor to the element edge should be longer than five times the embedment length of the anchor), the tensile membrane develops both in the horizontal and vertical directions. The tensile membrane's maximum extension was about five times the membrane thickness in the horizontal radial direction.
4. The tensile membrane's outer part, corresponding to 60% $R_{membrane}$, remained in the elastic domain during the loading process until pulling out of the threaded anchor.
5. No fracture of the UHPFRC substrate was observed; the failure of the anchorage occurred due to the widening of the inner part of the UHPFRC's annular circular tensile membrane and pulling out of the threaded anchor.

Supplementary Materials: The following supporting information can be downloaded at: https://www.mdpi.com/article/10.3390/buildings14113669/s1.

Author Contributions: Conceptualization, A.H. and E.B.; methodology, A.H. and E.B.; validation, A.H. and E.B.; formal analysis, A.H.; investigation, A.H.; writing—original draft preparation, A.H.; writing—review and editing, E.B.; supervision, E.B. All authors have read and agreed to the published version of the manuscript.

Funding: This research received no external funding.

Data Availability Statement: The data presented in this study are available in article.

Conflicts of Interest: The authors declare no conflicts of interest.

References

1. Hochuli, A.; Trouillet, J.-G.; Brühwiler, E.; Schulz, O.; Hoffmann, M. Renewal of a fixed railway track using UHPFRC—Part 2. *Bautechnik* **2022**, *99*, 10–17. [CrossRef]
2. Eligehausen, R.A.; Cook, R.; Appl, J. Behavior and Design of Adhesive Bonded Anchors. *ACI Struct. J.* **2006**, *103*, 822–831. [CrossRef]
3. Makita, T. Fatigue Behaviour of UHPFRC and R-UHPFRC—RC Composite Members. Thèse N°4848. Ph.D. Thesis, Swiss Federal Institute of Technology Lausanne (EPFL), Lausanne, Switzerland, 2010.
4. Shen, X. Static and Fatigue Biaxial Flexural Behavior of Strain-Hardening UHPFRC Thin Slab Elements. Thèse N°7460. Ph.D. Thesis, Swiss Federal Institute of Technology Lausanne (EPFL), Lausanne, Switzerland, 2020.

5. Oesterlee, C. Structural Response of Reinforced UHPFRC and RC Composite Members. Thèse N°6068. Ph.D. Thesis, Swiss Federal Institute of Technology Lausanne (EPFL), Lausanne, Switzerland, 2014.
6. Červenka Consulting s.r.o. *FEM Programm ATENA*, version 5.7.0; Červenka Consulting s.r.o.: Praha, Czech Republic, 2021.
7. Satoh, A.; Sakagami, Y.; Mitarai, S. Finite Element Analysis on Pull-out Behavior of Post-installed Adhesive Anchor Filled with UHPFRC. In Proceedings of the AFGC-ACI-Fib-RILEM International Conference on Ultra-High Performance Fibre-Reinforced Concrete, Montpellier, France, 2–4 October 2017.
8. Kalthoff, M.; Raupach, M. Pull—Out behaviour of threaded anchors in fibre reinforced ordinary concrete and UHPC for machine tool constructions. *J. Build. Eng.* **2020**, *33*, 101842. [CrossRef]
9. Fehling, E.; Lorenz, P. Characterisation of rebars anchorage in UHPC. In Proceedings of the RILEM-Fib-AFGC International Symposium on Ultra-High Performance Fibre-Reinforced Concrete, Marseille, France, 1–3 October 2013.
10. Grzesiak, S.; Pahn, M.; Schultz-Cornelius, M.; Susanne Bies, N. Influence of Different Fiber Dosages on the Behaviour of Façade Anchors in High-Performance Concrete. *CivilEng* **2021**, *2*, 556–579. [CrossRef]
11. Vita, N.; Sharma, A. Behaviour of single bonded anchors in uncracked steel fibre reinforced concrete under tensile loading—Experimental investigations and analytical model. *Eng. Struct.* **2023**, *288*, 116088. [CrossRef]
12. Pouraminian, M.; Akbari Baghal, A.E.; Andalibi, K.; Khosravi, F.; Arab Maleki, V. Enhancing the pull-out behavior of ribbed steel bars in CNT-modified UHPFRC using recycled steel fibers from waste tires: A multiscale finite element study. *Sci Rep.* **2024**, *14*, 19939. [CrossRef] [PubMed]
13. Zhao, H.; Wang, Y.; Liu, X.; Wang, X.; Chen, Z.; Lei, Z.; Zhou, Y.; Singh, A. Review on solid wastes incorporated cementitious material using 3D concrete printing technology. *Case Stud. Constr. Mater.* **2024**, *21*, e03676. [CrossRef]
14. He, L.; Chen, B.; Liu, Q.; Chen, H.; Li, H.; Chow, W.T.; Tang, J.; Du, Z.; He, Y.; Pan, J. A quasi-exponential distribution of interfacial voids and its effect on the interlayer strength of 3D printed concrete. *Addit. Manuf.* **2024**, *89*, 104296. [CrossRef]
15. Shu, J.; Zhang, X.; Li, W.; Zeng, Z.; Zhang, H.; Duan, Y. Point cloud and machine learning-based automated recognition and measurement of corrugated pipes and rebars for large precast concrete beams. *Autom. Constr.* **2024**, *165*, 105493. [CrossRef]
16. Chen, R.-S.; Zhang, H.-Y.; Hao, X.-K.; Yu, H.-X.; Shi, T.; Zhou, H.-S.; Wang, R.-B.; Zhao, Z.-F.; Wang, P. Experimental study on ultimate bearing capacity of short thin-walled steel tubes reinforced with high-ductility concrete. *Structures* **2024**, *68*, 107109. [CrossRef]
17. Hochuli, A.; Brühwiler, E. Numerical Simulation of the Structural Behavior of Threaded Anchors in UHPFRC. In Proceedings of the 3rd International Interactive Symposium on Ultra-High-Performance Concrete, Wilmington, DE, USA, 4–7 June 2023.
18. Hochuli, A.; Brühwiler, E. Failure Mechanism of Threaded Anchors in UHPFRC as Simulated by Finite Element Analysis. In Proceedings of the 4th International Symposium on Ultra-High Performance Fibre -Reinforced Concrete (UHPFRC), Menton, France, 21–23 October 2024.
19. Červenka, V.; Jendele, L.; Červenka, J. *ATENA Program Documentation Part 1, Theory*; Červenka Consulting s.r.o.: Prague, Czech Republic, 2021.
20. De Borst, R. *Non-Linear Analysis of Frictional Materials*; TU Delft: Delft, The Netherlands, 1986. Available online: https://resolver.tudelft.nl/uuid:d52ac7f8-d56f-4e0c-ab14-455ed02fcffe (accessed on 3 August 2023).
21. Cervenka, J.; Cervenka, V.; Laserna, S. On crack band model in finite element analysis of concrete fracture in engineering practice. *Eng. Fract. Mech.* **2018**, *197*, 27–47. [CrossRef]
22. Pukl, R.; Novák, D.; Sajdlová, T.; Lehký, D.; Červenka, J.; Červenka, V. Probabilistic design of fibre concrete structures. *IOP Conf. Ser. Mater. Sci. Eng.* **2017**, *246*, 012004. [CrossRef]

Disclaimer/Publisher's Note: The statements, opinions and data contained in all publications are solely those of the individual author(s) and contributor(s) and not of MDPI and/or the editor(s). MDPI and/or the editor(s) disclaim responsibility for any injury to people or property resulting from any ideas, methods, instructions or products referred to in the content.